Modeling Functional Dynamics of Cortical Gyri and Sulci

Xi Jiang[1](✉), Xiang Li[1], Jinglei Lv[1,2], Shijie Zhao[2], Shu Zhang[1],
Wei Zhang[1], Tuo Zhang[2], and Tianming Liu[1]

[1] Cortical Architecture Imaging and Discovery Lab,
Department of Computer Science and Bioimaging Research Center,
The University of Georgia, Athens, GA, USA
superjx2318@gmail.com
[2] School of Automation, Northwestern Polytechnical University, Xi'an, China

Abstract. Cortical gyrification is one of the most prominent features of human brain. A variety of studies in the brain mapping field have demonstrated the specific structural and functional differences between gyral and sulcal regions. However, previous studies of gyri/sulci function analysis based on the fMRI data assume the temporal stationarity over the entire fMRI scan, while the possible temporal dynamics of gyri/sulci function is largely unknown. We present a computational framework to model the functional dynamics of cortical gyri and sulci based on task fMRI data. Specifically, the whole-brain fMRI signals' temporal segments are derived via the sliding time window approach. The spatial overlap patterns among functional networks (SOPFNs), which are crucial for characterizing brain functions, are then measured within each time window via a group-wise sparse representation approach. Finally, the temporal dynamics of SOPFNs distribution on gyral/sulcal regions across all time windows are assessed. Experimental results based on the publicly released Human Connectome Project task fMRI data demonstrated that the proposed framework identified meaningful temporal dynamics difference of the SOPFNs distribution between gyral and sulcal regions which are reproducible across different subjects and task fMRI datasets. Our results provide novel understanding of functional dynamics mechanisms of human cerebral cortex.

Keywords: Cortical gyri and sulci · Functional dynamics · Spatial overlap pattern · Task-based fMRI

1 Introduction

Cortical gyrification, which is highly convoluted as convex gyri and concave sulci, is one of the most prominent characteristics of human brain [1]. A variety of studies have reported the specific structural/functional difference between gyral and sulcal regions. For example, from structural perspective, it is reported that the termination of streamline white matter fiber bundles derived from diffusion tensor imaging or high angular resolution diffusion imaging concentrate on gyrus in both human fetus and adult brains, as well as chimpanzee and macaque brains [2–4]. From functional perspective, a recent study reported that the functional connectivity based on resting state

functional magnetic resonance imaging (rsfMRI) data is strong between gyral-gyral regions, weak between sulcal-sulcal regions, and moderate between gyral-sulcal regions [5]. Another study demonstrated that the task-based heterogeneous functional regions derived from task fMRI (tfMRI) data locate significantly more on gyral regions than on sulcal regions [6].

Although significant progresses have been achieved in exploration of structural/functional difference between gyral and sulcal regions, a potential limitation is that previous studies of gyri/sulci function analysis based on the fMRI data (e.g., [5, 6]) assume the temporal stationarity over the entire fMRI scan, i.e., the functional measurement is performed over the entire fMRI scan, while the possible temporal dynamics of gyri/sulci function has been largely unknown. Neuroscience studies have suggested that the function of the brain is dynamic both spatially and temporally [7]. That is, the dynamically changing functional interactions between different cortical regions mediate the moment-by-moment functional switching in the brain [7]. Recent studies based on fMRI data also demonstrate that brain undergoes dynamical changes of functional connectivity [8]. In short, the investigation of possible functional dynamics difference between gyral and sulcal regions is crucial for understanding functional dynamic mechanisms of human cerebral cortex.

As an attempt to address the abovementioned limitation, in this work, we propose a computational framework to model the functional dynamics of cortical gyri and sulci based on task fMRI data. Firstly, the whole-brain fMRI signals' temporal segments are derived via the widely used sliding time window approach. Secondly, the spatial overlap patterns among functional networks (SOPFNs), which characterize the brain regions that are involved in multiple concurrent neural processes under specific task performance and has been demonstrated crucial in depicting brain functions [9, 10], are measured within each time window via the proposed group-wise sparse representation approach. Finally, based on the SOPFN distribution on gyral/sulcal regions within each time window, the temporal dynamics of SOPFN distribution on gyral/sulcal regions across all time windows are assessed. We hypothesize that there is functional dynamics (which is characterized by temporal dynamics of SOPFN distribution in this work) difference between cortical gyral and sulcal regions. Given the lack of ground-truth in brain mapping, we argue that the reproducibility across different subjects and tasks is a reasonable verification of the identified temporal dynamics difference of SOPFN distribution between cortical gyral and sulcal regions.

2   Materials and Methods

2.1   Data Acquisition and Pre-processing

The recently publicly released HCP (Q1 release) grayordinate tfMRI data [11] including 64 subjects and 7 task designs (emotion, gambling, language, motor, relational, social, and working memory) were used in this work. The tfMRI acquisition parameters and task designs are referred to [11]. Pre-processing of the tfMRI data was referred to [10]. Note that all subjects have the same number (64984) of 'grayordinates' (cortical surface vertices) [11] which have reasonably precise correspondences across subjects for group-wise analysis.

2.2   tfMRI Signals' Temporal Segments Extraction

The temporal segments of whole-brain tfMRI signals are firstly extracted for each subject as illustrated in Fig. 1. Specifically, for subject i, the tfMRI signals of whole-brain grayordinates were extracted, normalized to zero mean and standard deviation of 1, and aggregated into a signal matrix $X_i \epsilon \mathbb{R}^{t \times n}$ with t tfMRI time points and n grayordinates (Fig. 1a). The sliding time window approach, which has been widely and effectively applied for functional brain temporal dynamics analysis (e.g., [8]), is then adopted and defined in Eq. (1) to segment X_i into a series of consecutive temporal segments $X_i^{w_j} \epsilon \mathbb{R}^{l \times n}$ within the time window w_j which starts at time point t_j and has unified window length l:

$$X_i^{w_j} = \left\{ X_i^q | t_j \leq q \leq t_j + l, t_j = 1, .., (t - l + 1) \right\} \tag{1}$$

where X_i^q is the value of q-th row of X_i at time point q. There are $(t - l + 1)$ time windows in total for each subject.
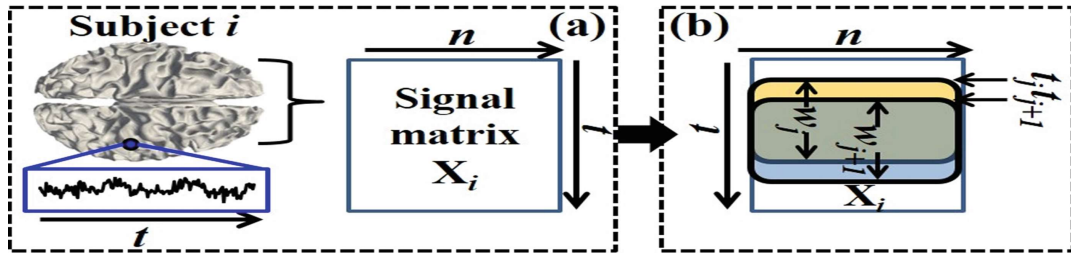

Fig. 1. tfMRI signals' temporal segments extraction. (a) The cortical surface and whole-brain tfMRI signal matrix X_i of subject i. The tfMRI signal of an example grayordinate (cortical vertex) is shown and highlighted by the blue frame. (b) Examples of extracted two consecutive temporal segments $X_i^{w_j}$ and $X_i^{w_{j+1}}$ (highlighted by yellow and blue frames, respectively).

2.3   SOPFN Identification via Group-Wise Sparse Representation of tfMRI Signal Temporal Segments

Based on the extracted tfMRI signals' temporal segments within each time window, we identify the SOPFN within each time window following the two major steps. First, we identify meaningful group-wise consistent functional networks across different subjects within each time window via a group-wise sparse representation approach. Second, we measure the SOPFN based on the identified functional brain networks within each time window.

The dictionary learning and sparse representation framework has been demonstrated to be efficient and effective in identifying concurrent functional brain networks from tfMRI signals [12, 13]. As illustrated in Fig. 2a, considering a group of I subjects, the temporal segment matrices $X_i^{w_j}$ at time window w_j of all subjects are arranged into a big matrix $X^{w_j} \epsilon \mathbb{R}^{l \times (n \times I)}$. X^{w_j} is then represented as an over-complete dictionary matrix
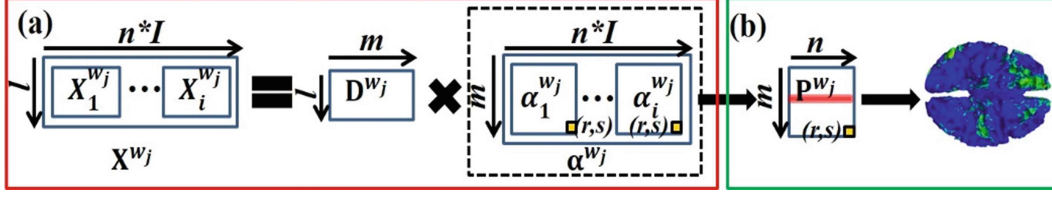
Fig. 2. (a) The illustration of group-wise sparse representation of temporal segments of a group of subjects. (b) An example identified group-wise consistent functional network via mapping a specific row (highlighted by red) of p^{w_j} back onto the cortical surface.

$D^{w_j} \epsilon \mathbb{R}^{l \times m}$ (m is the dictionary size, $m > l$ and $m \ll (n \times I)$) and a sparse coefficient weight matrix $\alpha^{w_j} \epsilon \mathbb{R}^{m \times (n \times I)}$ using an effective online dictionary learning algorithm [14]. In brief, an empirical cost function considering the average loss of regression to $n \times I$ temporal segments is defined as

$$f_{n \times I}(D^{w_j}) \triangleq \frac{1}{n \times I} \sum_{k=1}^{n \times I} \min_{\alpha_k^{w_j} \epsilon \mathbb{R}^m} \frac{1}{2} ||x_k^{w_j} - D\alpha_k^{w_j}||_2^2 + \lambda ||\alpha_k^{w_j}||_1 \qquad (2)$$

where ℓ_1-norm regularization and λ are adopted to trade-off the regression residual and sparsity level of $\alpha_k^{w_j}$. $x_k^{w_j}$ is the k-th column of X^{w_j}. To make the coefficients in α^{w_j} comparable, we also have a constraint for k-th column $d_k^{w_j}$ of D^{w_j} as defined in Eq. (3). The whole problem is then rewritten as a matrix factorization problem in Eq. (4) and solved by [14] to obtain D^{w_j} and α^{w_j}.

$$C \triangleq \left\{ D^{w_j} \epsilon \mathbb{R}^{l \times m} s.t. \forall\ k = 1, \ldots . m, (d_k^{w_j})^T d_k^{w_j} \leq 1 \right\} \qquad (3)$$

$$\min_{D^{w_j} C, \alpha^{w_j} \epsilon \mathbb{R}^{m \times (n \times I)}} \frac{1}{2} ||x_k^{w_j} - D^{w_j}\alpha_k^{w_j}||_2^2 + \lambda ||\alpha_k^{w_j}||_1 \qquad (4)$$

Since the dictionary learning and sparse representation maintain the organization of all temporal segments and subjects in X^{w_j}, the obtained α^{w_j} also preserve the spatial information of temporal segments across I subjects. We therefore decompose α^{w_j} into I sub-matrices $\alpha_1^{w_j}, \ldots, \alpha_i^{w_j} \epsilon \mathbb{R}^{m \times n}$ corresponding to I subjects (Fig. 2a). The element (r, s) in each sub-matrix represents the corresponding coefficient value of the s-th gray-ordinate to the r-th dictionary in D^{w_j} for each subject. In order to obtain a common sparse coefficient weight matrix across I subjects, we perform t-test of the null hypothesis for (r, s) across I subjects (p-value < 0.05) similar as in [15] to obtain the p-value matrix $p^{w_j} \epsilon \mathbb{R}^{m \times n}$ (Fig. 2b), in which element (r, s) represents the statistically coefficient value of the s-th grayordinate to the r-th dictionary across all I subjects. p^{w_j} is thus the common sparse coefficient weight matrix. From a brain science perspective, $d_k^{w_j}$ (k-th column of D^{w_j}) represents the temporal pattern of a specific group-wise consistent functional network and its corresponding coefficient vector $p_k^{w_j}$ (k-th row of p^{w_j}) can be mapped back to cortical surface (color-coded by z-score transformed from

p-value) (Fig. 2b) to represent the spatial pattern of the network. We then identify those meaningful group-wise consistent functional networks from $p_k^{w_j}$ ($k = 1, \ldots, m$) similar as in [10]. Specifically, the GLM-derived activation maps and the intrinsic networks templates provided in [16] are adopted as the network templates. The network from $p_k^{w_j}$ with the highest spatial pattern similarity with a specific network reference (defined as $J(S, T) = |S \cap T|/|T|$, S and T are spatial patterns of a specific network and a template, respectively) is identified as a group-wise consistent functional brain network at w_j.

Once we identify all group-wise consistent functional brain networks at w_j, the SOPFN at w_j is defined as the set of all common cortical vertices g_j ($i = 1..64984$) involved in the spatial patterns of all identified functional networks [9, 10]:

$$V_{w_j} = \forall g_i \text{ s.t. } g_i \text{ belongs to all networks at } w_j \tag{5}$$

2.4 Temporal Dynamics Assessment of SOPFN Distribution on Gyri/Sulci

Based on the identified SOPFN at time window w_j in Eq. (5), we assess the SOPFN distribution on cortical gyral/sulcal regions at w_j. Denote the principal curvature value of cortical vertex g_j ($i = 1..64984$) as $pcurv_{g_i} \begin{cases} \geq 0, g_i \in gyri \\ < 0, g_i \in sulci \end{cases}$ which is provided in HCP data [11], the SOPFN V_{w_j} on gyral and sulcal regions is represented as $V_{w_j|gyri} = \forall g_i \text{ s.t. } g_i \in V_{w_j}, pcurv_{g_i} \geq 0$, and $V_{w_j|sulci} = \forall g_i \text{ s.t. } g_i \in V_{w_j}, pcurv_{g_i} < 0$, respectively. Note that $V_{w_j} = V_{w_j|gyri} + V_{w_j|sulci}$. We further define the SOPFN distribution percentage at w_j as $P_{w_j|gyri} = |V_{w_j|gyri}|/|V_{w_j}|$ for gyri and $P_{w_j|sulci} = |V_{w_j|sulci}|/|V_{w_j}|$ for sulci, where $|.|$ denotes the number of members of a set and $P_{w_j|gyri} + P_{w_j|sulci} = 1$.

Finally, to assess the temporal dynamics of SOPFN distribution on gyral/sulcal regions, we define $P_{gyri} = \left[P_{w_1|gyri}, P_{w_2|gyri}, .., P_{w_j|gyri}\right]$. as a $(t - l + 1)$ dimensional feature vector representing the dynamics of SOPFN distribution percentage across all $(t - l + 1)$ time windows on gyri. Similarly, we define $P_{sulci} = \left[P_{w_1|sulci}, P_{w_2|sulci}, .., P_{w_j|sulci}\right]$ for sulci.

3 Experimental Results

For each of the seven tfMRI datasets, we equally divided all 64 subjects into two groups (32 each) for reproducibility studies. The window length l was experimentally determined ($l = 20$) using the similar method in [8]. The values of m and λ in Eq. (4) were experimentally determined ($m = 50$ and $\lambda = 1.5$) using the similar method in [13].

3.1   Group-Wise Consistent Functional Networks Within Different Time Windows

We successfully identified group-wise consistent functional networks within different time windows based on methods in Sect. 2.3. Figure 3 shows the spatial maps of two example identified functional networks within different time windows in one subject group of emotion tfMRI data. We can see that for each of the two networks (Figs. 3b–c), albeit similar in overall spatial pattern, there is considerable variability of the spatial pattern across different time windows compared with the network template. Quantitatively, the mean spatial pattern similarity J defined in Sect. 2.3 is 0.69 ± 0.10 and 0.36 ± 0.06 for the two networks, respectively. This finding is consistent between two subject groups for all seven tfMRI datasets. The spatial pattern variability of the same functional network across different time windows is in agreement with the argument that there is different involvement of specific brain regions in the corresponding networks across different time windows [7].
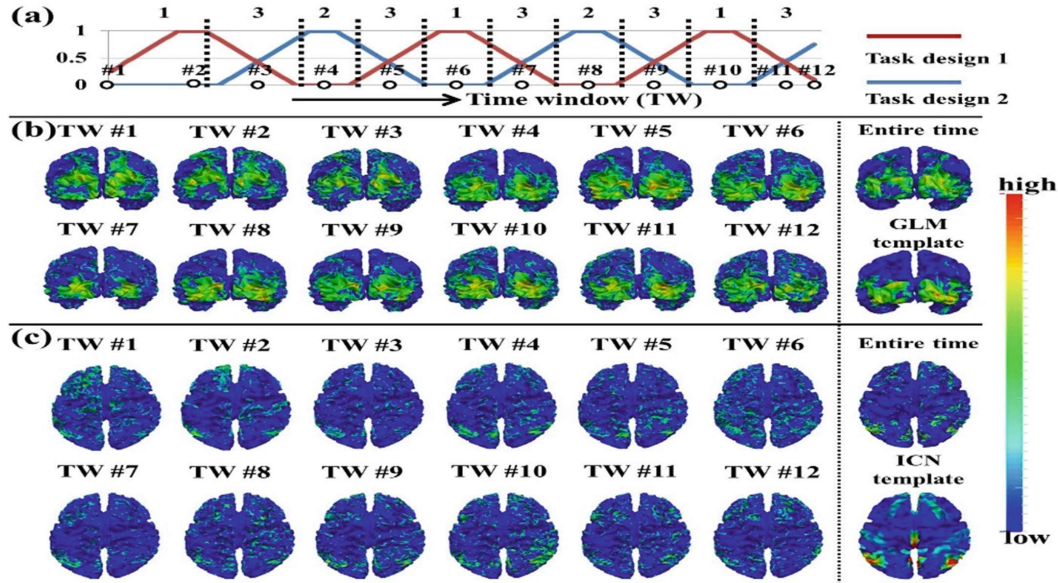

Fig. 3. Two example group-wise consistent functional networks within different time windows in one subject group of emotion tfMRI data. (a) Task design curves across time windows (TW) of emotion tfMRI data. 12 example TWs are indexed. Three different TW types are divided by black dashed lines and labeled. TW type #1 involves task design 1, TW type #2 involves task design 2, and TW type #3 involves both two task designs. The spatial patterns of (b) one example task-evoked functional network and (c) one example intrinsic connectivity network (ICN) within the 12 example TWs are shown.

3.2   Temporal Dynamics Difference of SOPFN Distribution on Gyri/Sulci

We identified the SOPFN based on all identified functional networks using Eq. (5) and further assessed the SOPFN distribution on cortical gyral/sulcal regions within each time window. Figure 4 shows the mean SOPFN distribution on gyri and sulci across
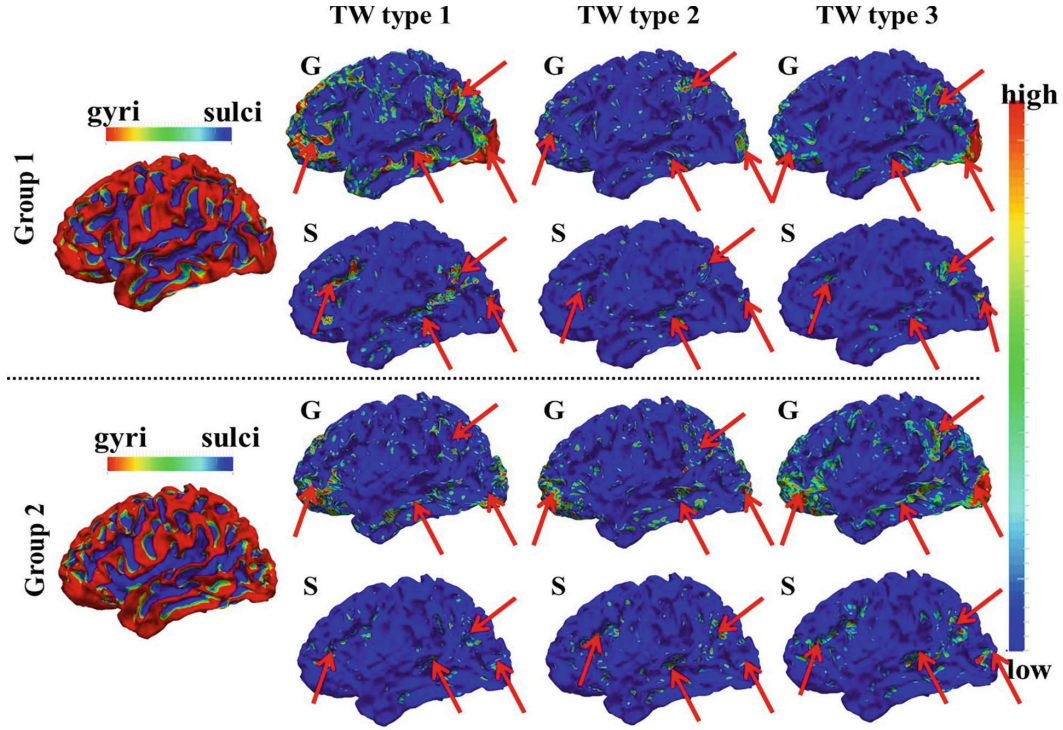
Fig. 4. The mean SOPFN distribution on gyral (G) and sulcal (S) regions across different time window types in the two subject groups of emotion tfMRI data. The common regions with higher density are highlighted by red arrows. The two example surfaces illustrate the gyri/sulci and are color-coded by the principal curvature value.

different TW types in emotion tfMRI data as example. We can see that albeit certain common regions (with relatively higher density as highlighted by red arrows), there is considerable SOPFN distribution variability between gyral and sulcal regions across different time windows. Quantitatively, the distribution percentage on gyral regions is statistically larger than that on sulcal regions across all time windows using two-sampled t-test (p < 0.05) for all seven tfMRI datasets as reported in Table 1.

Table 1. The mean ratio of SOPFN distribution percentage on gyri vs. that on sulci across all time windows in the two subject groups of seven tfMRI datasets.

	Emotion	Gambling	Language	Motor	Relational	Social	WM
Group 1	1.47	1.60	1.46	1.32	1.59	1.46	1.67
Group 2	1.45	1.55	1.38	1.33	1.49	1.47	1.66

Finally, we calculated and visualized P_{gyri} and P_{sulci} representing the dynamics of SOPFN distribution percentage across all time windows on gyri and sulci, respectively in Fig. 5. It is interesting that there are considerable peaks/valleys for the distribution percentage on gyri/sulci which are coincident with the specific task designs across the entire scan, indicating the temporal dynamics difference of SOPFN distribution between gyral and sulcal regions. These results indicate that gyri might participate
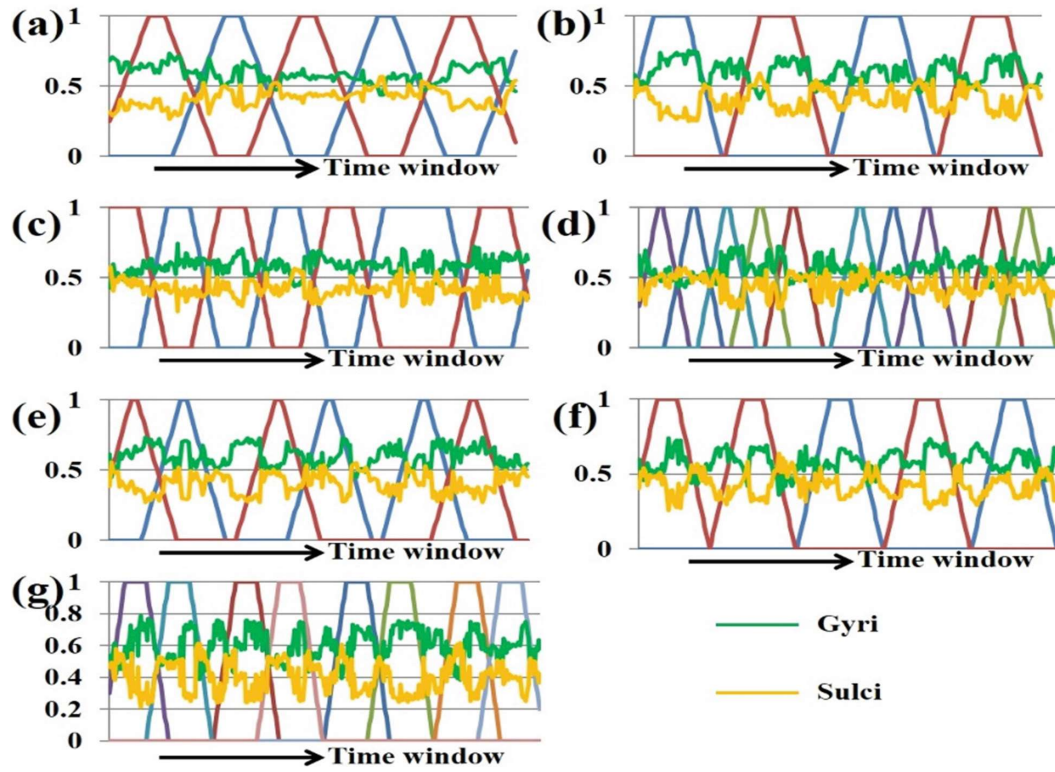
Fig. 5. The temporal dynamics of SOPFN distribution percentage on gyri (green curve) and sulci (yellow curve) across all time windows in the seven tfMRI datasets shown in (a)–(g), respectively. The task design curves in each sub-figure are represented by different colors. Y-axis represents the percentage value (*100 %).

more in those spatially overlapped and interacting concurrent functional networks (neural processes) than sulci under temporal dynamics. It should be noted that the identified temporal dynamics difference of SOPFN distribution between gyral and sulcal regions (Fig. 5) is reasonably reproducible between the two subject groups and across all seven high-resolution tfMRI datasets. Given the lack of ground truth in brain mapping, the reproducibility of our results is unlikely due to systematic artifact and thus should be a reasonable verification of the meaningfulness of the results.

4   Discussion and Conclusion

We proposed a novel computational framework to model the functional dynamics of cortical gyri and sulci. Experimental results based on 64 HCP subjects and their 7 tfMRI datasets demonstrated that meaningful temporal dynamics difference of SOPFN distribution between cortical gyral and sulcal regions was identified. Our results provide novel understanding of brain functional dynamics mechanisms in the future. We will investigate other potential sources of differences that are observed in the results in the future. We will apply the proposed framework on resting state fMRI data and more tfMRI datasets, e.g., the recent 900 subjects' tfMRI data released by HCP, to further reproduce and validate the findings.

References

1. Rakic, P.: Specification of cerebral cortical areas. Science **241**, 170–176 (1988)
2. Nie, J., et al.: Axonal fiber terminations concentrate on gyri. Cereb. Cortex **22**(12), 2831–2839 (2012)
3. Chen, H., et al.: Coevolution of gyral folding and structural connection patterns in primate brains. Cereb. Cortex **23**(5), 1208–1217 (2013)
4. Takahashi, E., et al.: Emerging cerebral connectivity in the human fetal brain: an MR tractography study. Cereb. Cortex **22**(2), 455–464 (2012)
5. Deng, F., et al.: A functional model of cortical gyri and sulci. Brain Struct. Funct. **219**(4), 1473–1491 (2014)
6. Jiang, X., et al.: Sparse representation of HCP grayordinate data reveals novel functional architecture of cerebral cortex. Hum. Brain Mapp. **36**(12), 5301–5319 (2015)
7. Gilbert, C.D., Sigman, M.: Brain states: top-down influences in sensory processing. Neuron **54**(5), 677–696 (2007)
8. Li, X., et al.: Dynamic functional connectomics signatures for characterization and differentiation of PTSD patients. Hum. Brain Mapp. **35**(4), 1761–1778 (2014)
9. Duncan, J.: The multiple-demand (MD) system of the primate brain: mental programs for intelligent behaviour. Trends Cogn. Sci. **14**(4), 172–179 (2010)
10. Lv, J.: Sparse representation of whole-brain fMRI signals for identification of functional networks. Med. Image Anal. **20**(1), 112–134 (2015)
11. Glasser, M.F., et al.: The minimal preprocessing pipelines for the Human Connectome Project. Neuroimage **80**, 105–124 (2013)
12. Lee, K., et al.: A data-driven sparse GLM for fMRI analysis using sparse dictionary learning with MDL criterion. IEEE Trans. Med. Imaging **30**(5), 1076–1089 (2011)
13. Lv, J., et al.: Holistic atlases of functional networks and interactions reveal reciprocal organizational architecture of cortical function. IEEE TBME **62**(4), 1120–1131 (2015)
14. Mairal, J., et al.: Online learning for matrix factorization and sparse coding. J. Mach. Learn. Res. **11**, 19–60 (2010)
15. Lv, J., et al.: Assessing effects of prenatal alcohol exposure using group-wise sparse representation of fMRI data. Psychiatry Res. **233**, 254–268 (2015)
16. Smith, S.M., et al.: Correspondence of the brain's functional architecture during activation and rest. Proc. Natl. Acad. Sci. U.S.A. **106**(31), 13040–13045 (2009)